Expedient Bayesian prediction of subfossil bone protein content using portable ATR-FTIR data

Sean Hixon [a,b,*], Patrick Roberts [a,c], Ricardo Rodríguez-Varela [d,e], Anders Götherström [d,e], Elena Rossoni-Notter [f], Olivier Notter [f], Pauline Raimondeau [g], Guillaume Besnard [g], Enrico Paust [h], Mary Lucas [a,i], Anna Lagia [j], Ricardo Fernandes [a,k,l,m]

[a] *Department of Archaeology, Max Planck Institute of Geoanthropology, Kahlaische Str. 10, 07745, Jena, Germany*
[b] *Department of Integrative Biology, Oregon State University, 2701 SW Campus Way, Corvallis, OR 97331 USA*
[c] *isoTROPIC Research Group, Max Planck Institute of Geoanthropology, Kahlaische Str. 10, 07745, Jena, Germany*
[d] *Centre for Palaeogenetics, 106 91, Stockholm, Sweden*
[e] *Department of Archaeology and Classical Studies, Stockholm University, 10691, Stockholm, Sweden*
[f] *Museum of Prehistoric Anthropology, 56 bis Bd du Jardin Exotique, 98000, Monaco*
[g] *CNRS, Université Paul Sabatier, IRD, Toulouse INP, UMR 5300, CRBE (Centre de Recherche sur la Biodiversité et l'Environnement), 118 Route de Narbonne, 31062, Toulouse, France*
[h] *Friedrich Schiller University of Jena, Chair of Prehistoric and Early Historical Archaeology, Löbdergraben 24A, 07743, Jena, Germany*
[i] *The Arctic University Museum of Norway, UiT-the Arctic University of Norway, N-9037, Tromsø, Norway*
[j] *Department of Archaeology, Ghent University, Belgium*
[k] *Arne Faculty of Arts, Masaryk University, Nováka a, 602 00, Brno, Czech Republic*
[l] *Climate Change and History Research Initiative, Princeton University, Princeton, USA*
[m] *University of Warsaw, Faculty of Archaeology, Department of Bioarchaeology, ul. Krakowskie Przedmieście 26/28, 00-927, Warszawa, Poland*

ARTICLE INFO

ABSTRACT

Rapid and minimally destructive methods for estimating the endogenous organic content of subfossil bone save time, lab consumables, and valuable ancient materials. Fourier transform infrared (FTIR) spectroscopy is an established method to estimate bone protein content, and portable spectroscopes enable field applications. We review the ability of benchtop and portable FTIR indices to predict %N and %collagen from 137 bone specimens drawn from eight taxa. We also explore associations of these indices with the endogenous DNA content estimated for 105 specimens. Bulk bone elemental abundance and crystallinity index data reflect diagenetic alteration of these specimens, which come from a variety of depositional environments in four countries (Madagascar, Greece, Monaco, and Germany). Infrared (IR) indices from benchtop and portable units perform similarly well in predicting observed sample N content and collagen yields. Samples that include little collagen (0–5 wt%) tend to have similar IR index values, and we present a Bayesian approach for the prediction of collagen yields. Bone type best explains variation in target species DNA content (endogenous DNA being particularly abundant in petrosals), but low IR index values were consistently associated with minimal DNA content. We conclude that, although portable FTIR fails to distinguish collagen preservation among poorly preserved samples, a simple approach with minimal sample preparation can effectively screen bone from a variety of taxa, elements, and environments for the extraction of organics.

1. Introduction

1.1. Motivation

Subfossil bone (i.e. ancient bone that is incompletely mineralized) is a valuable archive of paleoanthropological, palaeoecological, and paleoenvironmental information. The ^{14}C content of protein extracted from subfossil bone spanning the past ~55 ka often gives the most reliable estimate of when the given vertebrate died (Berger et al., 1964). Stable isotope analysis of subfossil protein contributes to inference

---

regarding paleoecology and past human activities (Burleigh and Broth-well, 1978). Additionally, ancient DNA (aDNA) may inform on past population movement and speciation (Baker et al., 2005; Larson et al., 2007). However, the extraction and purification of subfossil bone organics is labour- and time-consuming. Furthermore, some of the extraction techniques are highly destructive and are a concern for heritage protection (Díaz-Andreu, 2017). Because many bones include organics that are too degraded for analysis, it is useful both to focus investment on relatively promising specimens and to identify the minimum material required for analysis following a quantitative assessment of preservation.

Ancient bone specimens with promising preservation of proteins may be identified through visual inspection, chemical composition of an extracted subsample, or subsample energy absorption. Visual inspection can separate exceptionally well-preserved bones (high tensile strength, waxy luster, and concoidal fracture) from poorly preserved bones (porous, soft, and chalky). Yet this distinction has low precision (therefore not useful for selecting promising specimens when preservation is similar among specimens), and the accuracy of these estimates (how well the visually-assessed preservation matches actual preservation) is affected by observer bias and diverse forms of remineralization and other postmortem processes (Stafford et al., 1988). The weight percent nitrogen of bulk bone subsamples can help estimate protein content, which may vary across the length of a bone (fresh bone includes ~4% N by weight (Brock et al., 2012)). However, elemental analysis is relatively destructive when N is scarce, time consuming, and sensitive to exogenous N contamination (Lebon et al., 2016; Quiles et al., 2022). A minimally destructive alternative is to screen specimens according to how the bulk subfossil bone interacts with various wavelengths of infrared (IR) light.

1.2. IR background

Fourier Transform Infrared Spectroscopy (FTIR) uses incident and reflected infrared light to characterize the absorbance spectrum of a given material, which reflects the type of chemical bonds that are present in molecules of a given mixture. The mineral fraction of bone (bioapatite) contains phosphate (PO_4^{3-}) and carbonate (CO_3^{2-}), which include bonds that tend to preferentially absorb IR light with wavenumbers of ~1010 and ~1400 cm^{-1}, respectively. Other absorbance bands associated with PO_4^{3-} that are of particular interest for our study include those at ~600 and ~550 cm^{-1}. The organic fraction, mostly collagen protein, of bulk bone (~25% by weight of fresh bone) includes a diversity of bonds that form amides, which yield prominent IR absorption peaks at ~1641 cm^{-1} (due to C=O stretch, hereafter called A1 peak) and ~1542 cm^{-1} (due to N–H bend, hereafter called A2 peak). As subfossil bones lose endogenous organics such as collagen and DNA, traces of the amides diminish relative to those of bone minerals (Bouchard et al., 2019; Hollund et al., 2013; Lebon et al., 2016).

The simple ratio of A1/PO4 absorbance obtained from attenuated total reflectance (ATR) FTIR reliably predicts bone %N values (Lebon et al., 2016) and can be applied in the field both quickly and without destroying material (Quiles et al., 2022). Recent research has demonstrated further potential to use non-destructive shorter wavelength IR spectroscopy to infer bulk bone protein content (Sponheimer et al., 2019). Additionally, Chowdhury et al. (2021) use machine learning to identify particular spectrum attributes (e.g., the wavenumber of A1 absorption peak) that improve predictions of sample protein content (Table 1), and Malegori et al. (2023) use hyperspectral imaging to map collagen content in subfossil bones. Here, we focus on expedience and build on the work of Lebon et al. (2016) and several studies that compare portable and benchtop FTIR data (reviewed in Table 1) by introducing an user friendly approach for propagating uncertainty associated with IR-based collagen content predictions and illustrating this approach with IR data and collagen yields following two different pretreatment procedures applied to multiple bone types collected from a variety of environments (Table 1).

Table 1

Summary of published comparisons between the use of bulk bone powder IR spectra from benchtop and portable FTIR in predicting attributes of preserved bone organics.

Study		Bouchard et al. (2019)	Chowdhury et al. (2021)	Quiles et al. (2022)	This paper
Sample Origin		Italy	Italy France UK	Egypt Italy France Morocco	Madagascar Greece Germany Monaco
Instrument	Portable	Agilent 4500a Agilent Cary 630	Agilent 4500a	Bruker Alpha Thermo Nicolet iS5	Agilent 4300
	Benchtop	Perkin Elmer Spotlight 400 Perkin Elmer Spectrum 100 Agilent Cary 660	Bruker Opus Spectrometer PerkinElmer Spotlight 400	Bruker Vertex 70	Bruker Vertex 70
IR Proxy	A1/PO4	1		1	1
	Decision Tree		1		
Controls	Drilling	1	1	1	
	Anvil			1	
	Pressure				
Supporting Analysis	EA %N			1	1
	pXRF				1
	Wt. %Collagen				1
	Endogenous DNA		1		1
	ZooMS	1	1		
Burial Environ.	Cave	1	1	1	1
	Open Air		1	1	1
	Lacustrine				1
	Fluvial				1
Taxa	Non-human Mammals	1	1	1	1
	Humans			1	1
	Birds	1		1	1
	Reptiles				1
Bone Type	Petrous				1
	Carapace				1
	Other	1	1	1	1

1.3. Challenges

Despite the potential of ATR FTIR to help predict subfossil bone protein content, failed applications are known (King et al., 2011; Pestle et al., 2014; Presslee et al., 2021). These may follow from a combination of mismatches between the desired and actual sensitivity of the approach and also obstacles to reproducibility. The approach works when weight %N is greater than ~0.7 (Lebon et al., 2016), but there may be cases when samples with %N < 0.7 are of interest (Presslee et al., 2021). One of the limits on the sensitivity of the approach follows from an absorption peak from O–H bend (associated with structural water) around the A1 peak, which alters the A1/PO4 signal (Chadefaux et al., 2009).

Multiple variables affect the reproducibility of ATR FTIR measurements. While results are comparable between ATR FTIR and more traditional FTIR with potassium bromide pellets (Hollund et al., 2013), applied results are inconsistent across ATR FTIR machines (Bouchard et al., 2019). This variation among machines (following at least partly from differences in energy sources, detector types, and spectral resolutions) prevents direct application of a single set of equations to predict sample organic content from IR absorption spectra attributes (Bouchard et al., 2019; Lebon et al., 2016; Quiles et al., 2022). Additionally, even when using a single machine, absorption indices from triplicate measurements sometimes yield calculated estimates of collagen content that differ by > 10% (Lebon et al., 2016; Quiles et al., 2022). ATR IR spectra indices can be influenced by 1) the grain size distribution of powder applied to the ATR crystal (Hollund et al., 2013; Kontopoulos et al., 2018), 2) the anvil pressure on the ATR accessory plate (Lebon et al., 2016; Quiles et al., 2022), 3) variable atmospheric backgrounds (Quiles et al., 2022), and 4) differences in data processing, including peak selection and integration (Bouchard et al., 2019). Although it limits the expedience of the approach, some of these sources of noise can be controlled by multiple measurements, sieving powdered sample before analysis, using particular accessory plates that allow for refined control over anvil pressure (e.g. Golden Gate ATR accessory of Specac Ltd. (Lebon et al., 2016)), and using benchtop ATR FTIR under vacuum.

1.4. Goals

While the reproducibility of ATR FTIR measurements can be low, noise also exists in the process of extracting bone proteins (Fülöp et al., 2013). It is possible that variable success with protein extraction and purification has the practical consequence of diminishing the need for more refined ATR-based screening methods. Here, we test the extent to which ATR IR indices from multiple instruments can predict the weight percent nitrogen (wt. %N), the protein content (%protein), and %target species (endogenous) DNA of subfossil bones from a variety of archaeological and paleontological sites. To begin to explore the diverse diagenetic processes that affected the mineral fraction of our archaeological and paleontological bones, we examined infrared splitting factor (IRSF) values (sensitive to bioapatite crystallinity) and elemental abundances through portable X-ray fluorescence (pXRF, sensitive to dissolution, recrystallization, and permineralization). We review the generality of the use of portable and benchtop ATR FTIR data for predicting the preservation of bone organics by studying a great diversity of bone samples and using relatively few controls during sample preparation (Table 1). Additionally, we introduce a Bayesian approach to estimate collagen yields from instrument-specific IR data that propagates uncertainty associated with empirical relationships between IR indices and measures of collagen preservation.

2. Materials and methods

2.1. Samples

We selected 137 bone samples from past research on Madagascar (n = 61), Greece (n = 54), Monaco (n = 15), and Germany (n = 7) for analysis (Supplementary Data 1). The Madagascan samples come from both extinct herbivores [*Hippopotamus* sp. (n = 21), *Aldabrachelys* sp. (n = 14), and *Mullerornis modestus* (n = 2)] and introduced taxa [*Bos taurus indicus* (n = 13), *Ovis aries* (n = 7), and *Potamochoerus larvatus* (n = 3)]. The Monegasque samples from *Homo sapiens* (n = 7), *Bos* (n = 4), *Ovis* or *Capra* (n = 2), *Cervus elaphus* (n = 1), *Equus caballus* (n = 1), and an unidentified carnivore. With the exception of a red deer (*Cervus elaphus*) from Germany, the rest of the samples come from humans (*Homo sapiens*).

The ages of these samples span multiple intervals during the past ~5 ka and come from a diversity of depositional environments. The limited temporal spread is incidental, and the study could easily be applied to older specimens that include a range of organics preservation. Protein extracted from most of the Madagascan samples was previously directly ^{14}C dated (n = 53), and ages span between ~5 kya (*Aldabrachelys* sp., PSUAMS 8672, 5350 ± 25 ^{14}C BP) and recent centuries (*Bos taurus indicus*, PSUAMS 3617, 155 ± 15 ^{14}C BP) (Hixon et al., 2021, 2022). These bones come from 15 sites spread across SW Madagascar, and they were recovered from sediments in ponds (n = 29), floodplains (n = 6), open air contexts (n = 17), and caves (n = 7, with the remaining two specimens coming from unknown depositional environments). The Greek samples come from three ancient Athenian cemeteries (Kerameikos, Kotzia Square, and Laurion) dated to 2.6-2.0 kya (Karagiorga-Stathakopoulou, 1988; Kovacsovics, 1990; Lagia, 2015; Salliora-Oikonomakou, 1985; Stroszeck, 2014; Zachariadou and Kyriakou, 1993). Samples from Monaco come from a variety of different locales and from across a wide age range extending from the Bronze Age to the early modern period (~5.0-0.5 kya). Remaining samples come from a Bronze Age hill fort in Central Germany (Kuckenburg, likely ~5.3-3.1 kya), historic burials in Jena, Germany (Collegium, ~500-100 years old), and a modern deer bone collected near Jena. The latter specimen is the only fresh bone analyzed in this study and is meant to provide reference for comparison with data from ancient bone.

Bone powder used for analysis was collected during sampling (through sawing and cutting with a handheld Dremel rotary tool, and scraping with a scalpel) and was not sieved prior to analysis. Bones were cleaned only through manual scrapping before sampling, and specimens were handled with gloves in a fume hood during sampling to control the spread of fine powder. Small bone fragments and powder were stored in weighing paper or aluminium foil before analysis. This sampling was practically non-destructive as it used the leftover material from other processes, which was further powdered in some cases using a hand mortar and pestle that was wiped clean with 70% ethanol between samples. Most samples come from cortical bone, but the Madagascan samples also include carapace and plastron fragments (n = 10), petrosals (n = 5), and tooth dentine (n = 3).

2.2. ATR FTIR analysis

We gathered ATR FTIR data from all powdered bulk bone samples using both a Bruker Vertex 70X benchtop FTIR (bFTIR) with OPUS 7.5 software and an Agilent Technologies 4300 portable FTIR (pFTIR) with Microlab PC software housed in the laboratories of the Max Planck Institute of Geoanthropology in Jena, Germany. Approximately 1–2 mg of bulk bone powder was applied to cover the diamond in each case, the anvil was hand-tightened, and one IR spectrum was collected per sample. On the bFTIR, spectra were collected over 60 s with a resolution of 4 cm^{-1} and 64 scans in the range of 4000-400 cm^{-1}. The pFTIR collected 32 sample scans over 15 s across 2000-650 cm^{-1} with a resolution of 4 cm^{-1}. The diamond was cleaned with acetone between sample measurements. In the case of the bFTIR, we used a diamond ATR accessory plate and evacuated the sample compartment prior to each measurement. Data were acquired with the software OPUS (for bFTIR) and MicroLab PC (for pFTIR). Using the data acquisition software, backgrounds were removed automatically from pFTIR spectra and were

removed using 10 × rubberbanding from bFTIR spectra.

Based on PO_4^{3-} peaks observed across sample spectra (Fig. 1), we defined the PO_4^{3-} band as 1015-1024 cm^{-1} (bFTIR) and 1005-1029 cm^{-1} (pFTIR). We similarly defined the A1 band as 1636-1651 cm^{-1} (bFTIR) and 1640-1658 cm^{-1} (pFTIR). The A2 peak formed a clear local maximum only in the modern deer bone, and we defined the A2 band as 1539-1543 cm^{-1} in spectra from both FTIR units. When calculating indices, we used the maximum absorbance from each band. The infrared splitting factor (IRSF, Nielsen-Marsh and Hedges, 1997) is based on the two main peaks of the PO_4^{3-} v_4 vibrational mode and is defined by the sum of the absorbances at these peaks (595–605 & 555-570 cm^{-1}) divided by the local minimum absorbance between these peaks (582-594 cm^{-1}). The limited spectral range of the pFTIR means that IRSF values could be obtained only from the bFTIR (Fig. 1). Note that some ancient bone specimens (e.g. EASI 066 and EASI 069, both from the National Museum of Natural History, Paris) absorbed IR energy of ~1725 cm^{-1} and ~2950 cm^{-1}, which likely reflects C=O and C–H bonds, respectively, that are associated with polymers used to conserve museum specimens. Given that these bands are distinct from those of interest at lower wavenumbers and that exogenous soil organics are an even greater concern at lower wavenumbers, we chose to include the spectra with traces of conservants in our analysis.

2.3. Elemental analysis

Bone powder from all samples was massed into tin capsules for wt. % N analysis using a Thermo Fischer Elemental Analyzer at the Stable Isotope Research Laboratory of the Max Planck Institute of Geoanthropology (SIRL-MPI) in Jena, Germany. Calibrations were performed using measurements of an international reference material (USGS40 glutamic acid, ~9.5% N) and internal standard (C_6N_2, ~28.0% N).

Portable X-ray fluorescence (pXRF) data from all samples were gathered using a Thermo Scientific Niton XL3t analyzer mounted on a Niton mobile lead stand. Bone powder loaded on canisters (cylindrical, with base diameter of 7 mm and height of 20 mm) was analyzed for 180 s in triplicate using the small spot size setting to achieve sample depths of >1 cm. The mining Cu/Zn mode and factory calibration factors were used to convert energy spectra to elemental abundance data. Accuracy

was verified routinely through the analysis of certified reference materials from NIST, which included soil (SRM 2709a, "San Joaquin Soil") and metal (IARM 35 KN). Given that the mining Cu/Zn mode and reference materials do not match the matrix of our unknowns (bulk bone), the resulting pXRF data (reported in weight %) can be considered only semiquantitative (Hunt and Speakman, 2015).

2.4. Collagen extraction and analysis

Collagen was extracted and purified from all specimens aside from four Madagascan hippo petrous bones (n = 133, Hixon et al., 2022; Hixon et al., 2021). For the European samples, a standard method of purifying bone protein through EZEE filters has been previously described for the laboratory (Müller et al., 2022). Percent collagen yield estimates in this case compare residue mass following filtration to bulk bone mass prior to demineralization. The ancient Madagascan samples were purified using one of two different approaches: ultrafiltration (n = 50) and XAD resin column chromatography (n = 6). For these specimens, both crude gelatine yields (following gelatinization) and purified yields are recorded.

Elemental data from purified bone protein were previously gathered at the SIRL-MPI (for samples from Europe) and at both the Yale Analytical and Stable Isotope Center (YASIC) and the University of New Mexico's Center for Stable Isotopes (UNM-CSI). Purified bone protein atomic C:N ratio data are available for samples from Madagascar (n = 56), Greece (n = 53), and Germany (n = 7).

2.5. DNA extraction

Previous attempts to extract DNA from subsets of both the Greek samples (n = 51) and Madagascan samples (n = 54) make it possible to estimate the fraction of target species (endogenous) DNA that is present in each.

DNA molecules of Greek samples (n = 51) were extracted in the aDNA facilities at the Centre for Palaeogenetics (CPG), Stockholm University (Sweden). DNA extraction and library preparation were done as in (Rodríguez-Varela et al., 2023). Purified libraries were sequenced on NovaSeq 6000 at the SciLife Sequencing Centre in Stockholm. All samples were sequenced at varying read depths in a single lane, utilizing only one library per sample, except for the following cases: AL 10, for which we sequenced two different libraries across eight different lanes in varying proportions; AL 2 and AL 3, which consisted of two libraries sequenced in two different lanes; and AL 36, where the same library was sequenced in two different lanes. Sequencing reads were demultiplexed according to the pair of indexes of each sample sequence. Cutadapt v2.3 (Martin, 2011) was used for trimming adapters and FLASH v1.2.11 (Magoč and Salzberg, 2011) for merging of fastq reads. The reads were mapped against the human reference genome GRCh37 (hg19) using the Burrows-Wheeler Algorithm, as implemented by BWA v0.7.10, (Li and Durbin, 2009) with the following parameters: aln (-l 16500 -n 0.01 -o 2). A modified version of FilterUniqueSAMCons.py (Kircher, 2012) was used to condense the reads with identical start and end position into a consensus read. Finally, reads shorter than 35 base pairs and reads with less than 90% consensus with the reference are filtered out using percidentity_threshold.py (Skoglund et al., 2012). The presence of 3′ and 5′ cytosine deamination patterns characteristic of aDNA (Sawyer et al., 2012) was estimated using PMDtools (Skoglund et al., 2014). In Dataset S1, we report the proportion of C to T and G to A changes at the first and last base of each read, respectively. Note that for certain samples, there may not be a sufficient number of human reads to calculate the damage patterns with confidence. Therefore, we indicate when a sample has fewer than 10,000 filtered human reads available for damage pattern calculation. The human proportion was calculated by dividing the number of reads that mapped to the reference human genome (including only reads with a quality score of 30 or higher) by the total number of reads. For samples that were sequenced multiple times, both the human
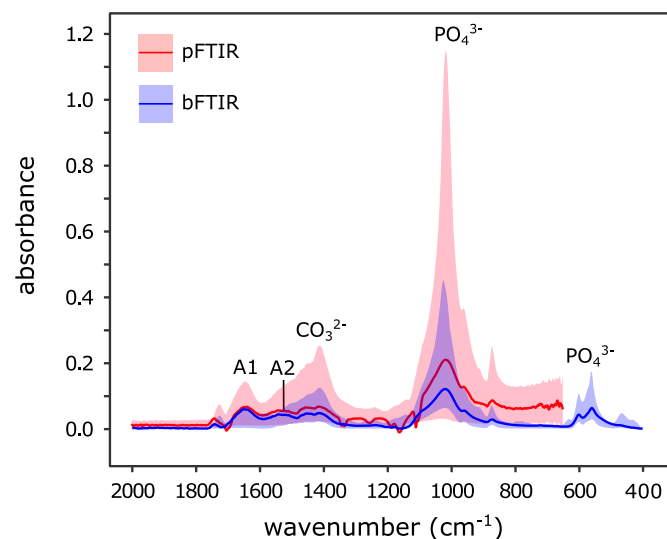

Fig. 1. Observed range of IR absorbance values in spectra from all bone powder samples analyzed with portable FTIR (pFTIR, red ribbon) and benchtop FTIR (bFTIR, blue ribbon). The solid lines give spectra from the modern deer bone analyzed with each machine, and the absorbance bands discussed in the text are labelled. Note the wide range of absorbance values explained by PO_4^{3-} and the difference in backgrounds at lower wavenumbers.

proportion and damage patterns were calculated as average values.

DNA extraction and genomic libraries of 54 Madagascan samples were prepared in the aDNA facilities of the Institute of Genomics of Tartu (Estonia), and sequencing was performed on an Illumina NextSeq 500 at the SNP & SEQ Technology Platform Sequencing of the Uppsala University (Sweden). Raw sequencing reads were then processed using the pipeline Paleomix v1.2.12 (Schubert et al., 2014). Adapter and low-quality bases were trimmed with AdapterRemoval v2 (Schubert et al., 2016), and overlapping reads collapsed. Reads shorter than 25 bp were discarded to avoid ambiguous mapping. Reads were then aligned to the most closely related nuclear genome available using BWA aln (seed disabled) v0.7.15 (Li and Durbin, 2009) in August 2021. For *Hippopotamus* sp. samples, we used as reference the genome of *Hippopotamus amphibius* (GCA_004027065.1). For *Aldabrachelys* sp., we used the giant turtle genome *Chelonoidis abingdonii* (GCF_003597395.1). The closest nuclear genome available for *Mullerornis modestus* and *Potamochoerus larvatus* are the kiwi (*Apteryx rowi*; GCF_003343035.1) and *Phacochoerus africanus*, respectively (GCA_016906955.1). Finally, we used the reference genomes for *Bos taurus* (GCA_000003205.6) and *Ovis aries* (GCA_000005525.1). Duplicate reads were removed with Picard Tools (https://broadinstitute.github.io/picard/). The endogenous DNA proportion was calculated by dividing the number of hits (regardless the mapping quality) by the total number of retained reads.

2.6. Data analysis

Regression analyses were completed in R version 4.0.3, and the R package glmulti (Calcagno and de Mazancourt, 2010) with the Akaike information criterion (AIC) helped to identify the most parsimonious variables to explain the observed variation in target species DNA yields (considering taxon, bone type, and site type as categorical predictors and wt. %N, conventional ^{14}C age, and bFTIR A1/PO4 as continuous

predictors). Box plots throughout illustrate interquartile ranges and whiskers that extend to maximum/minimum points that fall within 1.5 times the interquartile ranges. All data were made available through the Bone & Tooth Diagenesis data community on the Pandora data platform of the IsoMemo initiative (https://pandoradata.earth/organization /bone-tooth-diagenesis).

We employed a Bayesian log-linked regression model to establish the relationship between collagen yield and the IR ratio of the amide I peak vs. the phosphate peak: yield = A * log(A1/PO4) + B + ε, where A and B are regression parameters and ε is an error term centred at zero. All are normally distributed. The model was implemented using the Bpred R-based application developed within the Pandora & IsoMemo initiatives. The source code provides priors for parameter distributions and other modelling details (https://github.com/Pandora-IsoMemo/bpred/). The model was fitted using a Metropolis Hastings algorithm. Monte Carlo Markov Chain (MCMC) sampling settings (total number of iterations, burnin iterations, and number of MCMC chains) are fully described in a Bpred model file (https://pandora.earth/dataset/bulk-bone-ftir). Parameter posteriors can be sampled within Bpred to predict collagen yields from IR data.

3. Results

3.1. Sample preservation and burial conditions

Of the 23 elements detected in ancient bulk bone through pXRF, only three (P, S, & Ca) were detected in all specimens (n = 137). The modern deer bone included detections of only five additional elements (Cl, K, Ti, Cu, and Sr).

Of the five detected low-mass elements (Z < 19), Al was rarely detected (n = 2, both from Greece), Si was present in nearly half of the samples (n = 58, spread across all four countries), and Cl was commonly
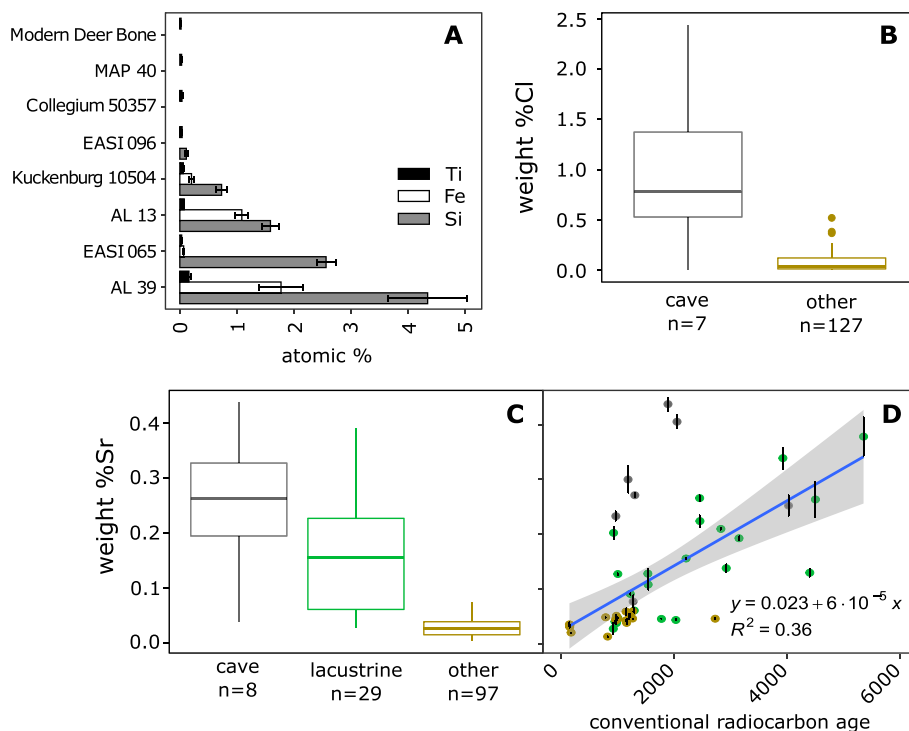

Fig. 2. Selected patterns of relative differences in bulk bone elemental abundance determined through pXRF. This includes (A) concentrations of silicon, iron, and titanium across select specimens (to highlight some of the range of variability), (B) greater abundance of chlorine in bones from coastal caves in Madagascar, (C) relatively abundant strontium in bones from caves and lacustrine deposits (also in Madagascar plus one Monegasque cave specimen), and (D) the general tendency for older samples to include more strontium (with adjusted r² shown). Note that only specimens from Madagascar that yielded directly ^{14}C-dated collagen are shown in frame D (lacustrine n = 23, cave n = 7, and other n = 21) and that the "other" category in this frame includes samples primarily from open air deposits. Whiskers in A and D represent 2σ ranges.

detected (n = 134). Samples with particularly abundant Si also tend to contain relatively large amounts of Fe and Ti (see Fig. 2A examples), and Cl tends to be comparatively abundant in bones collected from caves (Fig. 2B). Ratios of Ca/P range between 3.55 and 8.36, and median values from Madagascan, Greek, and Monegasque samples are significantly different (H(2) = 23.22, $p < 0.001$). Dunn's method of pairwise multiple comparisons suggests that the median Madagascan Ca/P value (m = 5.19, n = 61) is significantly larger than that of both the Greek samples (m = 4.85, n = 54, $p < 0.001$) and Monegasque samples (m = 4.88, n = 15, $p = 0.01$). Note that the median Collegium sample Ca/P value (4.47) and that from the modern deer (4.13) are apparently lower than those from specimens collected in Madagascar, Greece, and Monaco.

Of the 14 detected middle-mass elements (19 ≤ Z ≤ 41), seven were detected in over half of the analyzed samples (Ca, Ti, Cr, Fe, Cu, Zn, and Sr). Strontium tends to be relatively abundant both in specimens from dry caves and freshwater basins (Fig. 2C) and in older specimens (Fig. 2D). Of the middle-mass elements detected in less than half of the analyzed samples (K, V, Mn, As, Rb, Y, and Zr), only K was detected in bones from all four countries. Isolated detections included V (AL 39, a Greek sample) and Y (MAP 52, a Monegasque sample). Arsenic was detected only in Greek samples (n = 11), while Mn was detected primarily in Madagascan samples (n = 17, with another three detections in Greek samples). Rubidium detections (n = 18) were spread across specimens from all countries except Germany, and Zr detections were relatively rare [(in Greece (n = 3), and Monaco (n = 1)].

Of the four detected high-mass elements (41 < Z), only Ba and Pb were detected in specimens from more than one country. While Ba was otherwise detected in only one Monegasque specimen, Ba was detected in ~25% of the Madagascan samples (n = 16 of 61). Similarly, although Pb was otherwise detected in only three Monegasque specimens, Pb was detected in most Greek specimens (n = 46 of 54, ~85%). Pb estimates were particularly high in Greek specimens from Laurion (n = 6, 0.05–1.46%) relative to the rest of the Greek specimens (n = 48, 0.00–0.03%). Detections of Cd were limited to Greek bones (n = 3) and detections of U were limited to Madagascan bones (n = 2, both recovered from floodplain deposits near Ampoza).

3.2. Apatite crystallinity and protein

IRSF values range between 2.91 (EASI 053) to 5.59 (AL 17), and the modern deer bone has a value of 3.16. Median IRSF values from Madagascan, Greek, and Monegasque samples are significantly different (H(2) = 97.68, $p < 0.001$). Dunn's method of pairwise multiple comparisons suggests that the median IRSF values of specimens from Madagascar (m = 3.10, n = 61), Monaco (m = 3.40, n = 15), and Greece (m = 4.48, n = 54) are all significantly different ($p ≤ 0.009$). This contributes to the general observation that specimens collected from sediments exposed to the open air tend to have higher IRSF values (Fig. 3A).

Higher IRSF values tend to be associated with lower A1/PO4 values, with most of the variance in IRSF values confined to specimens with A1/PO4 < 0.1 (Fig. 3B). Although Mn abundance data are strongly positively skewed, note that specimens with higher IRSF values also tend to include more abundant Mn (Fig. 3C).

3.3. Collagen yield prediction

Within both the pFTIR and bFTIR datasets, bone A1/PO4 values range one order of magnitude. In the pFTIR dataset, these values range from 0.021 (AL 17) to 0.400 (EASI 063), and the modern deer bone has a value of 0.314. In the bFTIR dataset, A1/PO4 values range from 0.012 (AL 39) to 0.487 (modern deer bone). Given that the A2 peak was scarcely observed in IR spectra from both machines and that the range of A2/PO4 values is consistently small (pFTIR: 0.026–0.388, bFTIR: 0.032–0.453), we focus on A1/PO4 values as a proxy for sample protein content.

Bulk bone weight %N values range between 0.0 (MAP 52) and 4.9 (Collegium 50464), and the modern deer bone has a value of 3.6. Weight %N and A1/PO4 values are positively associated and highlight different tendencies for specimens collected from different countries (Fig. 4). Note that bFTIR A1/PO4 data explain a greater fraction of the variance in sample wt. %N values but that this difference is small (r^2 difference of 0.05).

Collagen yields from samples purified through EZEE filtration range between 0.0% (AL 43) and 28.4% (Collegium 50464) of the initial bulk bone mass before pretreatment, and the collagen yield from the modern deer bone is 22.0%. Yields from specimens purified through ultrafiltration (all from Madagascar) tend to be lower and less variable, with a range between 0.2% (EASI 095) and 15.7% (EASI 063). While bulk bone wt. %N values and collagen yields are positively associated, distributions of bulk bone wt. %N values from specimens in the different collagen yield categories overlap substantially (Fig. 5, collagen categories ranging from very low [red, 0–2%] to high [green, >10%]).
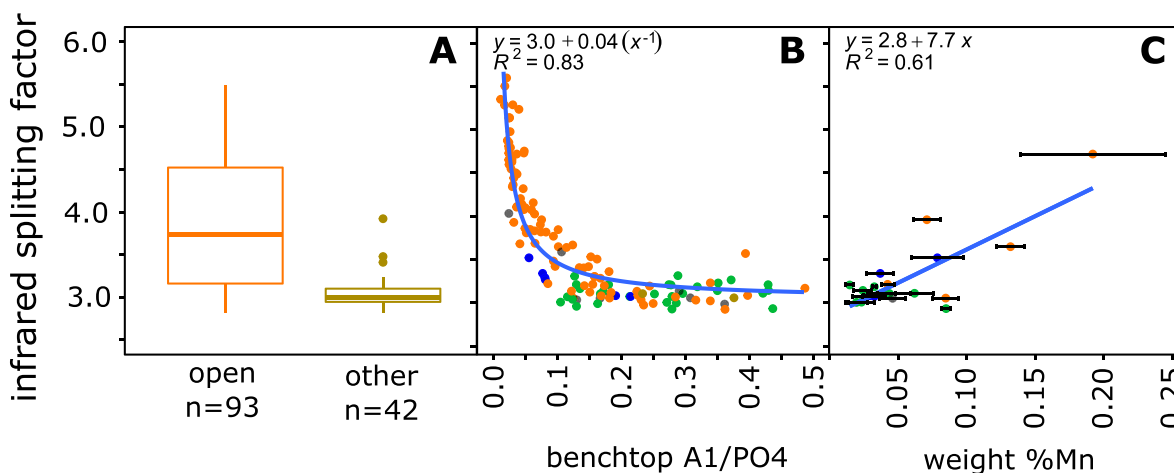

Fig. 3. Infrared splitting factor (IRSF) values from bFTIR analysis of bulk bone specimens as a function of (A) depositional environments, (B) bFTIR A1/PO4 values, and (C) weight %Mn estimated through pXRF, with whiskers to illustrate 2σ ranges (with adjusted r^2 value shown in each case). Frame B (n = 137) includes data from bone deposited in environments that include open air (orange, n = 92), lacustrine (green, n = 29), cave (grey, n = 8), fluvial (blue, n = 6), and unspecified (brown, n = 2). In frame C, the 20 specimens with Mn detection come from all site categories (lacustrine n = 10, open air n = 5, fluvial n = 4, and cave n = 1), and lines in this frame illustrate standard deviations around triplicate measurement means.
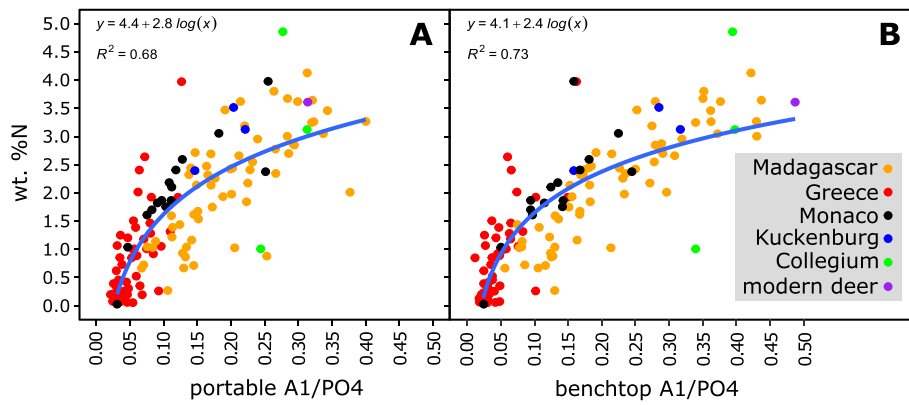
Fig. 4. Weight percent nitrogen as a function of bulk bone A1/PO4 values from (A) pFTIR, and (B) bFTIR. Logarithmic curves are fitted to each relationship (with adjusted r²), and points are colored according to geographic origin. The 137 points shown come from Madagascar (n = 61), Greece (n = 54), Monaco (n = 15), and Germany (n = 7, including Kuckenburg and Collegium).
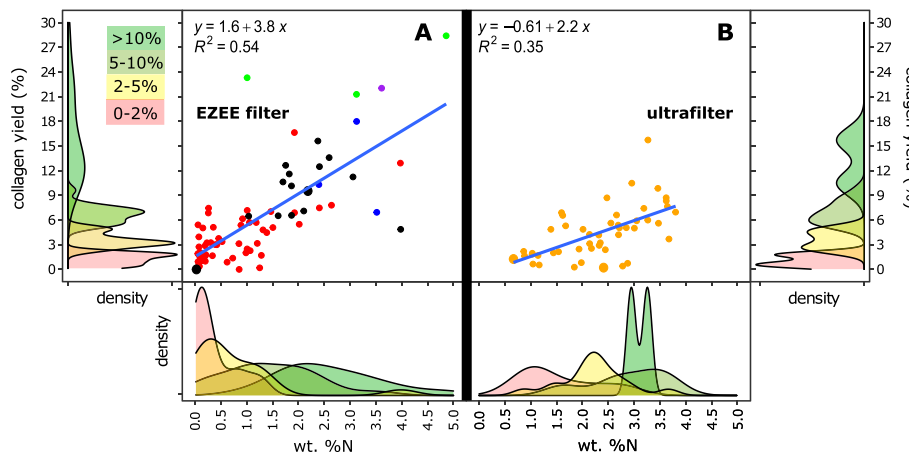

Fig. 5. Weight percent "collagen" yields through (A) EZEE filtration and (B) ultrafiltration as a function of bulk bone %N measurements (with adjusted r² shown). Points are colored according to geographic origin as in Fig. 4. The 124 points shown come from Greece (n = 54), Madagascar (n = 48), Monaco (n = 15), and Germany (n = 7). Densities separated and colored according to "collagen" yield groups (separated according to purification method) highlight the similarly low %N values of samples with different yields.
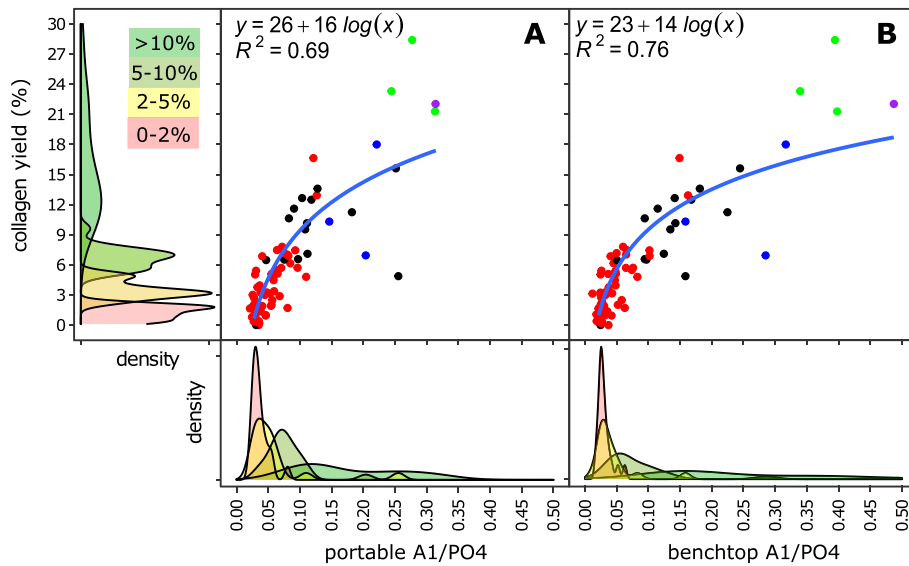

Fig. 6. Weight percent collagen yields as a function of bulk bone A1/PO4 values from (A) pFTIR and (B) bFTIR. Logarithmic curves are fitted to each relationship (with adjusted r²), and points are colored according to geographic origin as in Figs. 4 and 5. Densities separated and colored according to "collagen" yield groups highlight the similarly low A1/PO4 values of samples with different yields. The 76 points shown come from Greece (n = 54), Monaco (n = 15), and Germany (n = 7).

Both bFTIR and pFTIR A1/PO4 data fail to explain a greater fraction of the variance in ultrafiltered collagen yields. However, the IR data consistently explain a greater fraction of the variance in collagen yields following EZEE filtration (Fig. 6). The nonlinear relationship between A1/PO4 values and collagen yields means that samples with very poor collagen yields (red, 0–2%) and those with poor yields (yellow, 2–5%) have similar A1/PO4 values. Note that bFTIR A1/PO4 data explain more of the variance in collagen yield data than do pFTIR A1/PO4 data, but this difference is small. Fig. 7 illustrates the prediction of collagen yields based on bFTIR A1/PO4 through BPred. The two posterior distributions highlight that magnitude of the propagated uncertainty associated with a collagen yield estimate varies across the scale of possible A1/PO4 values.

3.4. Organic quality prediction

Of the 114 samples with collagen yield and atomic C:N data, 14 samples (all from Greece) have C:N > 3.5 (ranging from 4.2 to 8.1). These C:N values come from specimens with collagen yields that vary from very poor to moderate (up to 6.9% in the case of AL 4; Fig. 8A) and from specimens that fall within a narrow range of bulk bone pFTIR and bFTIR A1/PO4 values (0.02–0.04; Fig. 8B and C). Only about half of the samples with low A1/PO4 values had collagen quality that is sufficient for radiocarbon analysis. Specifically, only ~46% (12/26) of samples with pFTIR A1/PO4 < 0.04 yielded collagen with C:N ≤ 3.5. Similarly, only ~58% (20/34) of samples with bFTIR A1/PO4 < 0.04 yielded collagen with C:N ≤ 3.5.

Target species DNA yield estimates, for those samples with this information, range from 0.1% (EASI 046, *Aldabrachelys* sp.) to 85.0% (EASI 098, *Hippopotamus* sp.) of the total number of reads. All samples with target species DNA yields >4% (n = 19) are Madagascan. The bulk bone from these high yielding specimens has large ranges of wt. %N values (≥0.7), pFTIR A1/PO4 (≥0.105), and bFTIR A1/PO4 (≥0.128; Fig. 9). However, target species DNA estimates across taxa are predictably low (~1%) from specimens that fall outside these ranges of wt. %N, pFTIR A1/PO4, and bFTIR A1/PO4.

Proportions of 3′ and 5′ cytosine deamination among the Greek samples range from 0.000 (e.g., AL 33) to 0.371 (AL 42). Among all

Greek samples (n = 51), there is no relationship between endogenous DNA and bFTIR A1/PO4 (Fig. 10). However, among samples that include damage proportions >0.1 (n = 16), bFTIR A1/PO4 can explain a greater fraction of the variance in endogenous DNA estimates (r^2 = 0.1, as opposed to 0.0003 for Greek dataset in general).

Modelling endogenous DNA yields as a function of taxon, depositional environment, bone type (carapace, tooth root, petrosal, or other), bulk bone wt. %N, conventional ^{14}C age, and benchtop A1/PO4 values suggests that all of these variables (plus eight interaction terms) contribute to the most parsimonious model (AIC = 347.2, see Table S1 Model 1). A simple model that neglects interactions among explanatory variables (AIC = 384.2, Table S1 Model 2) suggests that DNA yields are particularly high among petrous bones (p = 0.001). Indeed, the petrous bones considered in this study (n = 5, all from extinct Madagascan hippos) have an average endogenous DNA yield of 70.3% (Fig. 9).

4. Discussion

Our results are consistent with existing research that supports that usefulness of both benchtop and portable ATR FTIR for estimating bulk bone collagen yields (Fig. 6, Lebon et al., 2016; Naito et al., 2020; Quiles et al., 2022). This result is particularly robust given that our study included both poor controls during ATR FTIR analysis (e.g., variable grain size and anvil pressure) and multiple bone types from a variety of depositional environments. As expected, our results suggest that the relationship between A1/PO4 values and collagen yields is largely independent of the diverse forms of diagenesis that contributed to the observed patterns of elemental abundance (Fig. 2) and bioapatite crystallinity (Fig. 3). The simple IR index predicts, admittedly poorly, target species DNA yields (Figs. 9 and 10) and collagen yields of <5% (Fig. 6). However, many samples with low collagen yields are of limited use given that they also have low collagen quality (Fig. 8), and A1/PO4 values may provide at least consistent cut-offs for separating samples with consistently low DNA yields.

4.1. Sample preservation and protein quality

Though semi-quantitative, elemental abundances estimated through pXRF reflect relative differences in diagenesis among the analyzed samples. The semiquantitative quality of the pXRF data (particularly for low-Z elements; (Shackley, 2011)) is clear through the observed range of Ca/P (3.55–8.36) and the value from our modern deer bone (4.13), which are both well above the expected value for modern bone (~2, Sillen, 1989; Woodard, 1962). Indeed, our P counts are consistently lower than the 7–12.5% estimated from a wide range of fresh human bones (Iyengar and Tandon, 1999). However, we do observe the expected relative pattern of older bones having higher Ca/P values, which likely follows from calcite mineralization during diagenesis. A detailed exploration of diagenetic changes in bone elemental abundance is beyond the scope of this study. We instead provide a few more general examples of relative differences with plausible explanations.

The positive association among Si, Ti, and Cr (Fig. 2A) likely follows from either silicate silt mixed with bone powder or from permineralization. Similarly, the relatively abundant Cl and Sr in samples from coastal caves may easily follow from water soluble salts deposited by sea spray (Fig. 2B and C). However, the enrichment of lacustrine bone in Sr likely follows from some combination of diffusion of Sr through pore waters into bioapatite lattice and substitution for Ca and authigenic formation of Sr-bearing apatite. The noisy but apparent dependence of Sr incorporation on time (Fig. 2D) suggests that Sr uptake is mostly independent of initial burial conditions. Indeed, Sr is not easily lost from subfossil bones (Tuross et al., 1989) and, based on the preferential incorporation of Ca in bioapatite, Turekian and Kulp (1956) suggest that Sr accumulation in bones could be used to establish relative chronology.

While both Sr and Pb also accumulate naturally in living bones (Comar et al., 1957; Iyengar and Tandon, 1999), additions following
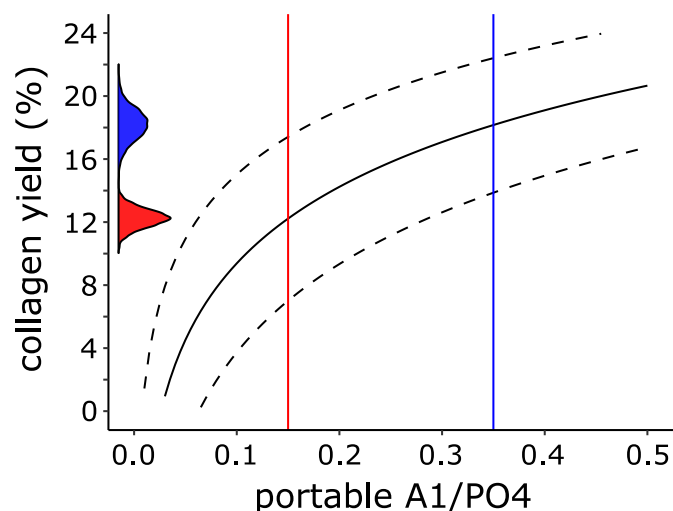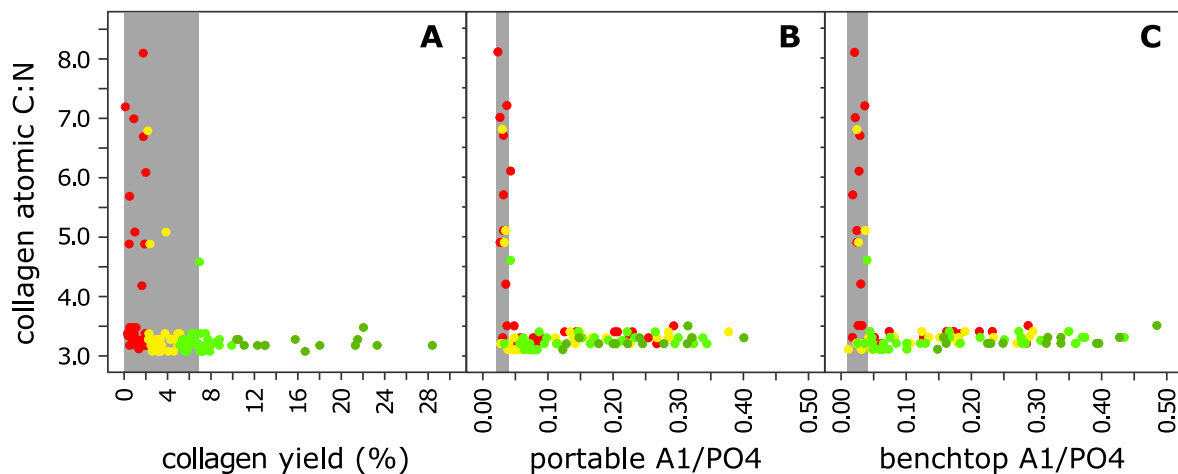

Fig. 7. Illustration of collagen yield estimate prediction from portable A1/PO4 through BPred. In this case, the equation of the line fit to data in Fig. 6A by BPred takes the form A * log(A1/PO4) + B, where A and B have estimates of 7.01 and 25.52, respectively (giving rise to the solid black curve), and A and B have 95% credible intervals of (5.90,8.09) and (22.36,28.60), respectively (giving rise to the dashed black curves). Color-coded lines and densities give examples of observed A1/PO4 values and uncertainty in predicted collagen yields.

Fig. 8. Collagen atomic C:N values as a function of (A) weight percent collagen yields and bulk bone A1/PO4 values from (B) pFTIR and (C) bFTIR. Points are colored according to collagen yield groups (see x-axis of frame A, as in density plots of Figs. 5 and 6). The 114 points shown come from Madagascar (n = 54), Greece (n = 53), and Germany (n = 7), and the shaded regions show the interval on each x-axis that include at least some samples with collagen C:N values greater than 3.5.
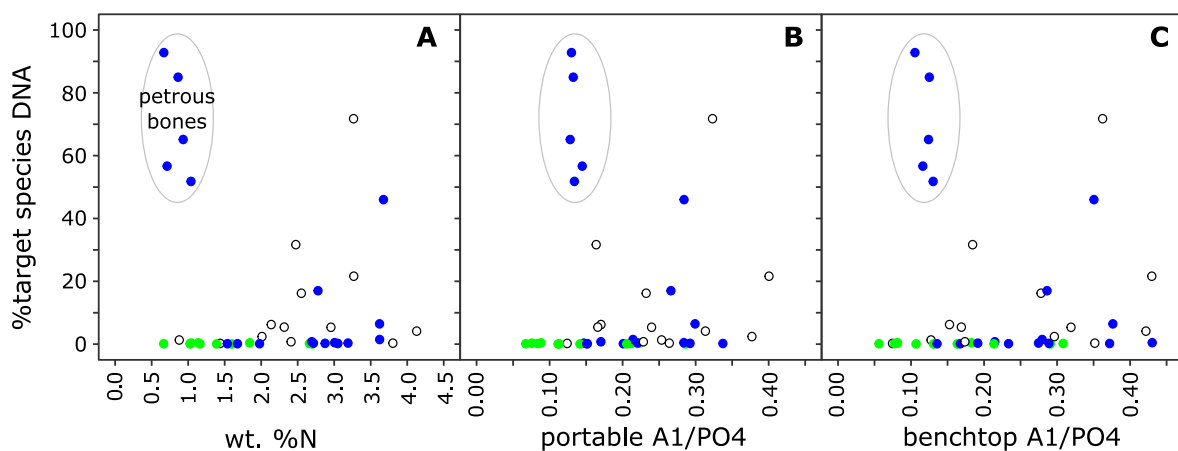

Fig. 9. Fraction of target species DNA in bones of Madagascan pygmy hippos (n = 21, blue), giant tortoises (n = 14, green), and zebu cattle (n = 13, white) as a function of bulk bone (A) weight %N and A1/PO4 values from (B) pFTIR and (C) bFTIR. Samples with target species DNA estimates come from Madagascan taxa with n > 10, and all five of the petrous bones used for analysis are circled in frame A.

burial can easily explain bones with abundant metallic elements. Indeed, bone mineral is used today to help immobilize metals in contaminated groundwater (Hodson et al., 2001; Ma et al., 1993). Consequently, the occasional detections of V, Y, Zr, and U are unsurprising, and the common detections of Pb in the Greek samples (and particularly abundant Pb in samples from Laurion) may follow from Pb released into groundwater during the ancient mining of silver-bearing lead ores such as galena and cerussite (Davis, 2014).

The growth of apatite crystals in most samples likely drives IRSF values > 3 (Fig. 3, Dal Sasso et al., 2018). The fact that bones from sites exposed to the open air have low Sr counts (Fig. 2C) yet high IRSF values (Fig. 3A) indicates that Sr accumulation and apatite crystal growth are not necessarily associated. Consequently, our data suggest 1) that recrystallization in open air bones occurs during interaction with low-Sr bearing water, and 2) that substitution of Sr for Ca in bioapatite most parsimoniously explains the accumulation of Sr in lacustrine bones. The widespread and consistent negative association between IRSF and A1/PO4 values is unexpected given that the relative rates of bone recrystallization and protein loss vary in theory among depositional environments (Trueman and Tuross, 2002). The non-linear relationship between IRSF and A1/PO4 values suggests that recrystallization detectable in IRSF values consistently occurs only after much loss of bone proteins.

The above-mentioned patterns are likely robust given that we did not consistently sample bone powder from a particular region of bone fragments. Indeed, the morphology of bones is known to affect the extent of diagenesis (Nielsen-Marsh and Hedges, 2000; Price et al., 1992), and sharp changes in elemental abundance profiles across bone sections demonstrate lasting patterns of heterogeneous remineralization (Fernandes et al., 2013; Trueman and Tuross, 2002). Zones of remineralization may in fact protect a bone's interior from the accumulation of elements such as Mn and the loss of the biogenic ^{14}C signal (Fernandes et al., 2013). We found suggestive evidence that IRSF values are positively associated with Mn uptake (Fig. 3C), but this pattern in bulk bones is not necessarily inconsistent with the finer scale analysis of Fernandes et al. (2013).

4.2. Prediction of collagen yield, collagen quality, and endogenous DNA yield

The positive correlations between bone collagen yield and recognized proxies of bone organic content (bulk bone %N and A1/PO4 values) are expected, as is the noise in relationships among these variables (Figs. 4–6). We present an application of a Bayesian regression model that helps to predict bone organic content while accounting for the observed uncertainty (Fig. 7). This appreciation for uncertainty aids
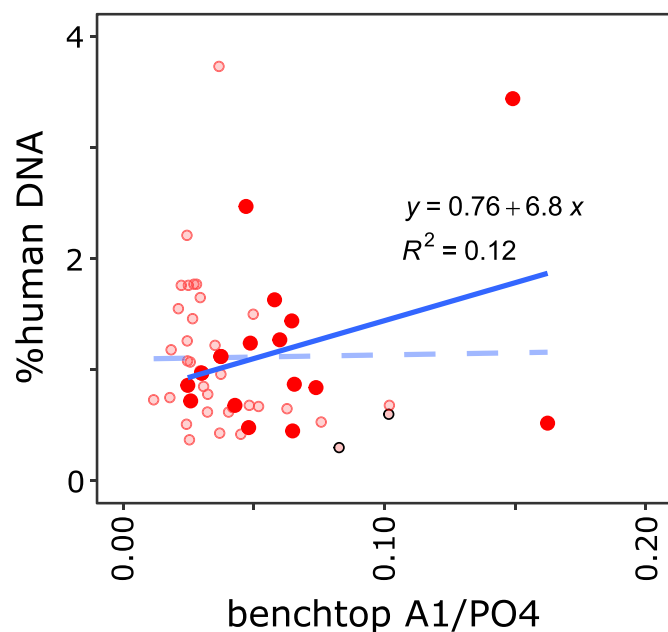
Fig. 10. Relationship between %human DNA and bulk bone A1/PO4 values for samples from Greece (n = 51), with points modified according to damage patterns: Large saturated red points mark specimens with damage estimates expected for ancient endogenous DNA (deamination proportions >0.1 for 3' and 5' cytosine, n = 16), small red points mark specimens with low damage estimates that likely follow from exogenous human DNA (n = 33), and small red points outlined in black (n = 2) mark specimens with high damage proportions yet both low numbers of filtered human reads (<5000) and atypical damage plots (Supplementary Dataset 1). The dashed blue line gives a linear fit to all data and that the solid blue line (with associated equation) is fit to data only from specimens with characteristic ancient endogenous DNA damage patterns. Note that bFTIR A1/PO4 values are shown and that pFTIR A1/PO4 values explain the same fraction of the variance in %human DNA values.

the accurate interpretation of IR index values. The uncertainty that we observed in the relationships between collagen yields and associated proxies is less than that observed in some studies (Naito et al., 2020) and more than those in others (e.g., Lebon et al., 2016; Quiles et al., 2022), where researchers both paid greater attention to reproducibility of FTIR analyses and focused on specimens from relatively few types of depositional environments. Inconsistency in our ATR IR index values follows from poorly constrained variables discussed in the Introduction, such as grain size distribution, anvil pressure, and atmospheric background. These easily explain why the observed relationships in Figs. 4 and 6 do not match the equations reported by Lebon et al. (2016). Given these limitations and observed differences with past studies, it is significant that 1) A1/PO4 values from pFTIR and bFTIR perform similarly well in predicting wt. %N and collagen yield values, and 2) data from both FTIR units explain a greater fraction of the variance in collagen yields than does the wt. %N data.

Noise in the observed relationships among bone protein proxies follows partly from wt. %N measurements. The presence of exogenous N (e.g., from soil nitrates and amino acids) in bulk bones diminishes the connection between bulk bone %N and protein content. This may explain why some old bones (e.g., Collegium 50464, with wt. %N = 4.9) has a higher fraction of N than the modern deer bone (3.6% N). Reproducibility of %N measurements may also be low [±0.3%, as reported for replicates in the case of Lebon et al. (2016)], which possibly explains why our modern deer bone appears to have less N than is typically reported for modern bone (~4%, Iyengar and Tandon, 1999; Lebon et al., 2016). These sources of error also help explain why wt. %N values underperform A1/PO4 values in predicting EZEE filter collagen yields (Fig. 5A and 6).

It is important to note that, although "collagen" yield is a measure of practical interest, it is also an approximation of the true protein content of a bone (Martínez Cortizas and López-Costas, 2020). This explains why the large range of A1/PO4 values in the Madagascan samples (Fig. 4) is not matched by a similarly large range of ultrafiltered collagen yields (Fig. 5; relative to the EZEE filtered collagen yields). Purified collagen yields evidently vary according to pretreatment type, and the exclusion of the <30 kDa fraction in the ultrafiltered collagen yields diminishes collagen yields to the point that they are difficult to predict through %N and A1/PO4 values. Conversely, inflated collagen yields may follow from the presence of exogenous salts forming during pretreatment involving weak acids and bases. This may explain why some collagen yields from old bones (e.g., Collegium 50464, with yield of 28.4%) are greater than that from the modern deer bone (22.0%, comparable to previous estimates from modern bones (Van Klinken, 1999)).

While A1/PO4 values fail to distinguish between bones with low to negligible collagen yields (Fig. 6), the practical consequence of this is diminished by the fact that many collagen samples from low-yielding bones are too poorly preserved to permit reliable stable isotope and ^{14}C analysis (with C:N > 3.5, Fig. 8, or collagen yield <1%, Van Klinken, 1999). It is possible that the increased spread of IRSF values among bones with A1/PO4 < 0.1 (Fig. 3A) give an opportunity to use crystallinity to predict collagen yields. However, within this subset of data, IRSF values explain a smaller fraction of the variance in collagen yields than do bFTIR A1/PO4 values.

The observation that hippo petrosals include particularly abundant target species DNA is consistent with research involving ancient human petrous bones and is likely explained by the low porosity of these bones (Hansen et al., 2017; Pinhasi et al., 2015). In the case of the human (Greek) specimens, the presence of exogenous human DNA, with minimal damage, is likely the reason why bFTIR A1/PO4 values explain a greater portion of the variance in human DNA yields within the subset of samples containing relatively high damaged DNA. Many other variables explain small fractions of the variance in DNA yields, which is consistent with a review that found some dependence of DNA yields on collagen yields, C/P values, and apatite crystallinity (Tamara et al., 2022). We generally found the preservation of target species DNA and bone proteins to be poorly associated across taxa (Fig. 9). However, similar to cut-offs proposed in past studies (Kontopoulos et al., 2020; Tamara et al., 2022), our data do at least suggest that non-petrous bones with A1/PO4 < 0.15 and wt. %N < 1.0 are difficult candidates for DNA extraction.

5. Conclusions

Using subfossil bones from a variety of taxa, skeletal elements, geographic locations, and depositional environments, we review the practicality and limitations of expedient approaches to predicting bone collagen content through portable and benchtop FTIR. This diversity allowed us to corroborate and expand on previous work that has also investigated the relationship between protein preservation and IR spectra under more constrained sample conditions.

If confronted with a large and highly diverse collection of ancient bone fragments, a researcher interested in extracting organics for ^{14}C and stable isotope analysis can quickly identify relatively promising specimens to focus extraction effort by first checking A1/PO4 values from crudely sampled powder on a portable or benchtop FTIR. The effects of such screening on the resulting chemical datasets must be carefully considered in the context of a given research question given that it can represent a source of bias. Our research highlights that quantitative estimates of collagen yield depend largely on collagen extraction protocols and to some extent on FTIR instrumentation. A researcher interested in such estimates can use samples with a range of collagen preservation to establish a protocol-specific calibration curve (e.g., Fig. 6), generate collagen yield estimates from the A1/PO4 values of unknowns, and propagate the associated uncertainty using BPred (e.g., Fig. 7). Such an approach does not make it possible to distinguish

among samples with low collagen yield estimates (<5%), some of which may nonetheless be of interest given that they include organics suitable for isotopic analysis. Similar quantitative estimates of DNA preservation based on IR indices are not possible, but cutoffs in A1/PO4 values may help identify groups of bones that are more or less promising for DNA extraction.

Data availability

All data generated through this study are available in the article supplementary material. These data are also available through the Bone & Tooth Diagenesis data community on the Pandora data platform of the IsoMemo initiative (https://pandoradata.earth/organization/bone-tooth-diagenesis).

CRediT authorship contribution statement

Sean Hixon: Conceptualization, Formal analysis, Investigation, Methodology, Project administration, Visualization, Writing – original draft, Writing – review & editing. **Patrick Roberts:** Funding acquisition, Resources, Supervision, Writing – review & editing. **Ricardo Rodríguez-Varela:** Investigation, Writing – review & editing. **Anders Götherström:** Funding acquisition, Investigation, Writing – review & editing. **Elena Rossoni-Notter:** Resources, Writing – review & editing. **Olivier Notter:** Resources, Writing – review & editing. **Pauline Raimondeau:** Investigation, Writing – review & editing. **Guillaume Besnard:** Funding acquisition, Investigation, Writing – review & editing. **Enrico Paust:** Resources, Writing – review & editing. **Mary Lucas:** Investigation, Writing – review & editing. **Anna Lagia:** Resources, Writing – review & editing. **Ricardo Fernandes:** Conceptualization, Data curation, Formal analysis, Investigation, Methodology, Project administration, Resources, Supervision, Writing – review & editing.

Declaration of competing interest

The authors declare that they have no known competing financial interests or personal relationships that could have appeared to influence the work reported in this paper.

Appendix A. Supplementary data

Supplementary data to this article can be found online at https://doi.org/10.1016/j.quaint.2024.05.002.

References

Baker, A.J., Huynen, L.J., Haddrath, O., Millar, C.D., Lambert, D.M., 2005. Reconstructing the tempo and mode of evolution in an extinct clade of birds with ancient DNA: the giant moas of New Zealand. Proc. Natl. Acad. Sci. USA 102 (23), 8257–8262.

Berger, R., Horney, A.G., Libby, W., 1964. Radiocarbon dating of bone and shell from their organic components. Science 144 (3621), 999–1001.

Bouchard, G.P., Mentzer, S.M., Riel-Salvatore, J., Hodgkins, J., Miller, C.E., Negrino, F., Buckley, M., 2019. Portable FTIR for on-site screening of archaeological bone intended for ZooMS collagen fingerprint analysis. J. Archaeol. Sci.: Reports 26, 101862.

Brock, F., Wood, R., Higham, T.F., Ditchfield, P., Bayliss, A., Ramsey, C.B., 2012. Reliability of nitrogen content (% N) and carbon: nitrogen atomic ratios (C: N) as indicators of collagen preservation suitable for radiocarbon dating. Radiocarbon 54 (3–4), 879–886.

Burleigh, R., Brothwell, D., 1978. Studies on Amerindian dogs, 1: carbon isotopes in relation to maize in the diet of domestic dogs from early Peru and Ecuador. J. Archaeol. Sci. 5 (4), 355–362.

Calcagno, V., de Mazancourt, C., 2010. glmulti: an R package for easy automated model selection with (generalized) linear models. J. Stat. Software 34 (12), 1–29.

Chadefaux, C., Le Hô, A.-S., Bellot-Gurlet, L., Reiche, I., 2009. Curve-fitting micro-ATR-FTIR studies of the amide I and II bands of type I collagen in archaeological bone materials. e-Preservation Sci. 6, 129–137.

Chowdhury, M.P., Choudhury, K.D., Bouchard, G.P., Riel-Salvatore, J., Negrino, F., Benazzi, S., Harrison, R., 2021. Machine learning ATR-FTIR spectroscopy data for the screening of collagen for ZooMS analysis and mtDNA in archaeological bone. J. Archaeol. Sci. 126, 105311.

Comar, C., Russell, R.S., Wasserman, R., 1957. Strontium-calcium movement from soil to man. Science 126 (3272), 485–492.

Dal Sasso, G., Asscher, Y., Angelini, I., Nodari, L., Artioli, G., 2018. A universal curve of apatite crystallinity for the assessment of bone integrity and preservation. Sci. Rep. 8 (1), 1–13.

Davis, G., 2014. Mining Money in Late Archaic Athens. Historia: Zeitschrift fuer Alte Geschichte 63 (3), 257–277.

Díaz-Andreu, M., 2017. Heritage Values and the Public, vol. 4. Taylor & Francis, pp. 2–6.

Fernandes, R., Hüls, M., Nadeau, M.-J., Grootes, P.M., Garbe-Schönberg, C.-D., Hollund, H.I., Kienle, L., 2013. Assessing screening criteria for the radiocarbon dating of bone mineral. Nucl. Instrum. Methods Phys. Res. Sect. B Beam Interact. Mater. Atoms 294, 226–232.

Fülöp, R.-H., Heinze, S., John, S., Rethemeyer, J., 2013. Ultrafiltration of bone samples is neither the problem nor the solution. Radiocarbon 55 (2), 491–500.

Hansen, H.B., Damgaard, P.B., Margaryan, A., Stenderup, J., Lynnerup, N., Willerslev, E., Allentoft, M.E., 2017. Comparing ancient DNA preservation in petrous bone and tooth cementum. PLoS One 12 (1), e0170940.

Hixon, S.W., Domic, A.I., Douglass, K.G., Roberts, P., Eccles, L., Buckley, M., Kennett, D. J., 2022. Cutmarked bone of drought-tolerant extinct megafauna deposited with traces of fire, human foraging, and introduced animals in SW Madagascar. Sci. Rep. 12 (1), 18504.

Hixon, S.W., Douglass, K.G., Crowley, B.E., Rakotozafy, L., Clark, G., Anderson, A., Kennett, D., 2021. Late Holocene spread of pastoralism coincides with endemic megafaunal extinction on Madagascar. Proc. Roy. Soc. Lond. B 288 (1955), 20211204.

Hodson, M., Valsami-Jones, E., Cotter-Howells, J., Dubbin, W., Kemp, A., Thornton, I., Warren, A., 2001. Effect of bone meal (calcium phosphate) amendments on metal release from contaminated soils—a leaching column study. Environ. Pollut. 112 (2), 233–243.

Hollund, H., Ariese, F., Fernandes, R., Jans, M., Kars, H., 2013. Testing an alternative high-throughput tool for investigating bone diagenesis: FTIR in attenuated total reflection (ATR) mode. Archaeometry 55 (3), 507–532.

Hunt, A.M., Speakman, R.J., 2015. Portable XRF analysis of archaeological sediments and ceramics. J. Archaeol. Sci. 53, 626–638.

Iyengar, G.V., Tandon, L., 1999. Minor and Trace Elements in Human Bones and Teeth.

Karagiorga-Stathakopoulou, T., 1988. Δημόσια έργα και ανασκαφές στην Αθήνα τα τελευταία πέντε χρόνια. ΗΟΡΟΣ 6, 87–108.

King, C.L., Tayles, N., Gordon, K.C., 2011. Re-examining the chemical evaluation of diagenesis in human bone apatite. J. Archaeol. Sci. 38 (9), 2222–2230.

Kircher, M., 2012. Analysis of high-throughput ancient DNA sequencing data. Ancient DNA: methods and protocols 197–228.

Kontopoulos, I., Penkman, K., Mullin, V.E., Winkelbach, L., Unterländer, M., Scheu, A., Teasdale, M.D., 2020. Screening archaeological bone for palaeogenetic and palaeoproteomic studies. PLoS One 15 (6), e0235146.

Kontopoulos, I., Presslee, S., Penkman, K., Collins, M.J., 2018. Preparation of bone powder for FTIR-ATR analysis: the particle size effect. Vib. Spectrosc. 99, 167–177.

Kovacsovics, W.K., 1990. Die Eckterrasse an der Gräberstrasse des Kerameikos. Kerameikos Ergebnisse der Ausgrabungen vol. XIV..

Lagia, A., 2015. Diet and the polis: an isotopic study of diet in Athens and Laurion during the Classical Hellenistic and Emperial Roman Periods. (Vol. Hesperia Sup. 49, 119–145. Hesperia Sup.

Larson, G., Cucchi, T., Fujita, M., Matisoo-Smith, E., Robins, J., Anderson, A., Kim, T.-H., 2007. Phylogeny and ancient DNA of Sus provides insights into neolithic expansion in Island Southeast Asia and Oceania. Proc. Natl. Acad. Sci. USA 104 (12), 4834–4839.

Lebon, M., Reiche, I., Gallet, X., Bellot-Gurlet, L., Zazzo, A., 2016. Rapid quantification of bone collagen content by ATR-FTIR spectroscopy. Radiocarbon 58 (1), 131–145.

Li, H., Durbin, R., 2009. Fast and accurate short read alignment with Burrows–Wheeler transform. Bioinformatics 25 (14), 1754–1760.

Ma, Q.Y., Traina, S.J., Logan, T.J., Ryan, J.A., 1993. In situ lead immobilization by apatite. Environ. Sci. Technol. 27 (9), 1803–1810.

Magoč, T., Salzberg, S.L., 2011. FLASH: fast length adjustment of short reads to improve genome assemblies. Bioinformatics 27 (21), 2957–2963.

Malegori, C., Sciutto, G., Oliveri, P., Prati, S., Gatti, L., Catelli, E., Mazzeo, R., 2023. Near-infrared hyperspectral imaging to map collagen content in prehistoric bones for radiocarbon dating. Commun. Chem. 6 (1), 54.

Martin, M., 2011. Cutadapt removes adapter sequences from high-throughput sequencing reads. EMBnet. journal 17 (1), 10–12.

Martínez Cortizas, A., López-Costas, O., 2020. Linking structural and compositional changes in archaeological human bone collagen: an FTIR-ATR approach. Sci. Rep. 10 (1), 17888.

Müller, L.M., Kipnis, R., Ferreira, M.P., Marzo, S., Fiedler, B., Lucas, M., Roberts, P., 2022. Late Holocene dietary and cultural variability on the Xingu River, Amazon Basin: a stable isotopic approach. PLoS One 17 (8), e0271545.

Naito, Y.I., Yamane, M., Kitagawa, H., 2020. A protocol for using attenuated total reflection Fourier-transform infrared spectroscopy for pre-screening ancient bone collagen prior to radiocarbon dating. Rapid Commun. Mass Spectrom. 34 (10), e8720.

Nielsen-Marsh, C.M., Hedges, R.E., 1997. Dissolution experiments on modern and diagenetically altered bone and the effect on the infrared splitting factor. Bull. Soc. Geol. Fr. 168 (4), 485–490.

Nielsen-Marsh, C.M., Hedges, R.E., 2000. Patterns of diagenesis in bone I: the effects of site environments. J. Archaeol. Sci. 27 (12), 1139–1150.

Pestle, W.J., Ahmad, F., Vesper, B.J., Cordell, G.A., Colvard, M.D., 2014. Ancient bone collagen assessment by hand-held vibrational spectroscopy. J. Archaeol. Sci. 42, 381–389.

Pinhasi, R., Fernandes, D., Sirak, K., Novak, M., Connell, S., Alpaslan-Roodenberg, S., Raczky, P., 2015. Optimal ancient DNA yields from the inner ear part of the human petrous bone. PLoS One 10 (6), e0129102.

Presslee, S., Penkman, K., Fischer, R., Richards-Slidel, E., Southon, J., Hospitaleche, C.A., MacPhee, R., 2021. Assessment of different screening methods for selecting palaeontological bone samples for peptide sequencing. J. Proteonomics 230, 103986.

Price, T.D., Blitz, J., Burton, J., Ezzo, J.A., 1992. Diagenesis in prehistoric bone: problems and solutions. J. Archaeol. Sci. 19 (5), 513–529.

Quiles, A., Lebon, M., Bellot-Gurlet, L., Bickel, S., 2022. ATR-FTIR pre-screening analyses for determining radiocarbon datable bone samples from the Kings' Valley, Egypt. J. Archaeol. Sci. 139, 105532.

Rodríguez-Varela, R., Moore, K.H., Ebenesersdóttir, S.S., Kilinc, G.M., Kjellström, A., Papmehl-Dufay, L., Kashuba, N., 2023. The genetic history of scandinavia from the roman iron age to the present. Cell 186 (1), 32–46. e19.

Salliora-Oikonomakou, M., 1985. Αρχαίο νεκροταφείο στην περιοχή Λαυρίου. ArchDelt 40, Aʹ, pp. 90–132.

Sawyer, S., Krause, J., Guschanski, K., Savolainen, V., Pääbo, S., 2012. Temporal patterns of nucleotide misincorporations and DNA fragmentation in ancient DNA. PLoS One 7 (3), e34131.

Schubert, M., Ermini, L., Sarkissian, C.D., Jónsson, H., Ginolhac, A., Schaefer, R., McCue, M., 2014. Characterization of ancient and modern genomes by SNP detection and phylogenomic and metagenomic analysis using PALEOMIX. Nat. Protoc. 9 (5), 1056–1082.

Schubert, M., Lindgreen, S., Orlando, L., 2016. AdapterRemoval v2: rapid adapter trimming, identification, and read merging. BMC Res. Notes 9 (1), 1–7.

Shackley, M.S., 2011. An introduction to X-ray fluorescence (XRF) analysis in archaeology *X-ray fluorescence spectrometry*. XRF) in Geoarchaeology. Springer, pp. 7–44.

Sillen, A., 1989. Diagenesis of the inorganic phase of cortical bone. The chemistry of prehistoric human bone 211–229.

Skoglund, P., Malmström, H., Raghavan, M., Storå, J., Hall, P., Willerslev, E., Jakobsson, M., 2012. Origins and genetic legacy of Neolithic farmers and hunter-gatherers in Europe. Science 336 (6080), 466–469.

Skoglund, P., Northoff, B.H., Shunkov, M.V., Derevianko, A.P., Pääbo, S., Krause, J., Jakobsson, M., 2014. Separating endogenous ancient DNA from modern day contamination in a Siberian Neandertal. Proc. Natl. Acad. Sci. USA 111 (6), 2229–2234.

Sponheimer, M., Ryder, C.M., Fewlass, H., Smith, E.K., Pestle, W.J., Talamo, S., 2019. Saving old bones: a non-destructive method for bone collagen prescreening. Sci. Rep. 9 (1), 1–7.

Stafford, T.W., Brendel, K., Duhamel, R.C., 1988. Radiocarbon, 13 C and 15 N analysis of fossil bone: removal of humates with XAD-2 resin. Geochem. Cosmochim. Acta 52 (9), 2257–2267.

Stroszeck, J., 2014. Der Kerameikos in Athen: Geschichte, Bauten und Denkmäler im archäologischen Park. Bibliopolis.

Tamara, L., Irena, Z.P., Ivan, J., Matija, Č., 2022. ATR-FTIR spectroscopy as a pre-screening technique for the PMI assessment and DNA preservation in human skeletal remains–A review. Quat. Int.

Trueman, C.N., Tuross, N., 2002. Trace elements in recent and fossil bone apatite. Rev. Mineral. Geochem. 48 (1), 489–521.

Turekian, K.K., Kulp, J.L., 1956. Strontium content of human bones. Science 124 (3218), 405–407.

Tuross, N., Behrensmeyer, A.K., Eanes, E., 1989. Strontium increases and crystallinity changes in taphonomic and archaeological bone. J. Archaeol. Sci. 16 (6), 661–672.

Van Klinken, G.J., 1999. Bone collagen quality indicators for palaeodietary and radiocarbon measurements. J. Archaeol. Sci. 26 (6), 687–695.

Woodard, H.Q., 1962. The elementary composition of human cortical bone. Health Phys. 8 (5), 513–517.

Zachariadou, O., Kyriakou, D., 1993. Πλατεία Κοτζιά. ArchDelt 43 (Βʹ1), 22–29, 1988.